

Emergent facilitation behavior in a distinguishable-particle lattice model of glass

Ling-Han Zhang^{1,*} and Chi-Hang Lam^{1,†}

¹*Department of Applied Physics, Hong Kong Polytechnic University, Hong Kong, China*
(Dated: April 25, 2022)

We propose an interacting lattice gas model of structural glass characterized by particle distinguishability and site-particle-dependent random nearest-neighboring particle interactions. This incorporates disorder quenched in the configuration space rather than in the physical space. The model exhibits non-trivial energetics while still admitting exact equilibrium states directly constructible at arbitrary temperature and density. The dynamics is defined by activated hopping following standard kinetic Monte Carlo approach without explicit facilitation rule. Kinetic simulations show emergent dynamic facilitation behaviors in the glassy phase in which motions of individual voids are significant only when accelerated by other voids nearby. This provides a microscopic justification for the dynamic facilitation picture of structural glass.

I. INTRODUCTION

Glassy dynamics still admits many open questions despite decades of intensive studies¹⁻³. When supercooled below the glass transition temperature T_g , many liquids can be quenched into the glassy phase, an amorphous solid-like state without long-range order. Molecular dynamics (MD) simulations are able to capture the dramatic slowdown^{4,5}, but a thorough understanding of the simulated dynamics also proves challenging. The study of simplified lattice models⁶⁻¹³ is thus important. In particular, the p-spin model⁷ has inspired the random first-order transition (RFOT) theory^{14,15}, a leading theory of glass. A potential issue in the p-spin model however is that it assumes externally imposed quenched disorder rather than the expected self-generated disorder, although a density functional Hamiltonian with self-generated disorder has also been used to demonstrate RFOT¹⁶. Another promising theory is dynamic facilitation¹⁷⁻¹⁹ founded on kinetically constrained models (KCM)^{8,9}. An important example is a spin-facilitation model by Fredrickson and Andersen (FA) in which defects interpreted as low-density regions are allowed to evolve only when facilitated by the presence of adjacent defects⁸. A full microscopic justification of the facilitation rules still remains a challenge.

In this work, we formulate a distinguishable-particle lattice model (DPLM), which is a lattice gas model with effectively infinitely many particle-types. This generalizes other multi-species models for glass^{4,12,20}. It also models glassy systems in which most particles have distinct properties including polymers⁵, polydisperse colloidal systems²¹ and monodisperse systems in which particle interactions admit random positional shifts²²⁻²⁴. More generally, it is suggested to model also identical-particle glassy systems in which distinct particle properties effectively account for the positional disorder of particles at sub-lattice resolutions. DPLM can be simulated at arbitrary temperature and particle density realizing physical systems ranging from dilute gases to glasses. Interestingly, the glassy phase exhibits dynamic facilitation as an emergent property.

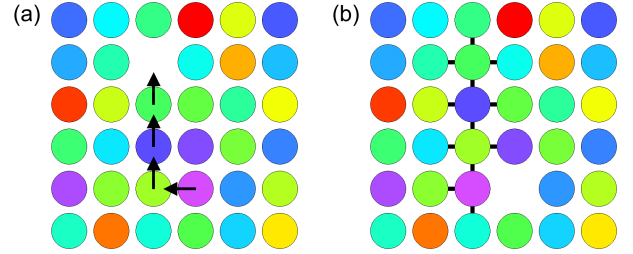


FIG. 1. (a) Schematic diagram of a region with distinguishable particles randomly colored. The arrows indicate a possible sequence of hops by four particles arranged in a line. The dynamics is equivalently described by four hops of a single void in the reversed direction. (b) The particle displacements alter the nearest neighbor pairings and hence the pair interactions (indicated by black lines) along the *whole* path.

II. MODEL

DPLM is defined by N particles on a 2D square lattice of unit lattice constant and size L^2 with periodic boundary conditions. No more than one particle can occupy each site. Each particle is distinguishable from the others (see Fig. 1). For an occupied site i , the particle index $s_i = 1, 2, \dots, N$ denotes which particle is at site i . For convenience, we let $s_i = 0$ if the site is unoccupied, i.e. occupied by a void. The occupation number n_i is hence

$$n_i = 1 - \delta_{s_i, 0} \quad (1)$$

where δ is the Kronecker delta. The whole set of s_i , rather than n_i , uniquely specifies the state of our system.

The total system energy is defined as

$$E = \sum_{\langle i, j \rangle} V_{ij s_i s_j} n_i n_j \quad (2)$$

where the sum is over all nearest neighboring (NN) sites. It can be equivalently written as

$$E = \sum_{\langle i, j \rangle'} V_{ij s_i s_j} \quad (3)$$

where the sum is restricted to bonded NN sites i and j , i.e. with both sites occupied by particles.

A key feature is the site-particle-dependent interaction energy V_{ijkl} . Its dependence on particle indices k and l means that each particle defines its own interaction strengths and this will be justified further. Effectively, each particle is a type of its own generalizing multi-species models. In DPLM, each V_{ijkl} is time-independent and is an independent variable following a probability distribution $g(V_{ijkl})$ except when the symmetry $V_{ijkl} = V_{jilk}$ applies. We expect V_{ijkl} to be bounded below as in typical two particle interactions and thus $g(V_{ijkl})$ should not be for example a simple Gaussian. For simplicity, $g(V_{ijkl})$ is assumed to be the uniform distribution in $[-0.5, 0.5]$ which leads to a particle interaction slightly attractive on average.

To better understand the time-dependence of the interactions, it is instructive to write Eq. (3) as

$$E = \sum_{\langle i,j \rangle'} V_{ij}(t) \quad (4)$$

where $V_{ij}(t) \equiv V_{ij s_i s_j}$. We emphasize that while each interaction V_{ijkl} for any given sites i and j and particles k and l is a quenched random variable, the interaction $V_{ij}(t)$ at site i and j and arbitrary particles is *not* quenched. Instead, $V_{ij}(t)$ admits an implicit time dependence via s_i and s_j , which are time dependent and change in values when a particle at i or j is replaced. Equally importantly, $V_{ij}(t)$ has no explicit time dependence. A previous value can thus be exactly reinstated whenever a previous local particle configuration as specified by s_i and s_j is restored via the return of the particles. We believe that such particle-dependent local interactions with persistent memory capture essential characteristics of structural glass. A further subtle point is that since $V_{ij}(t)$ depends on time, the disorder in our model is *not* quenched in the physical space, unlike spin-glass models⁶. Instead, because of the time independence of V_{ijkl} and that the same interaction energy always applies to the same local particle configuration, the disorder is quenched in the configuration space.

This site-particle dependence in V_{ijkl} is not necessarily due to possible diverse particle properties. Instead, it effectively account for the impacts of positional disorder at sub-lattice resolutions which are usually truncated in lattice models. A particle at site i in a spatially disordered system in principle admits a small random offset $\Delta \mathbf{r}_i$ from the exact lattice point. This results in a random deviation in the atomic separation \mathbf{r}_{ij} between the particles at sites i and j and hence also in the pair interaction V_{ijkl} . Rather than explicitly modeling the disorder in $\Delta \mathbf{r}_i$ or \mathbf{r}_{ij} , we directly consider the resulting random fluctuations in the interaction by simply taking a random V_{ijkl} . The dependence on both site and particle indices models the random changes expected to be induced by the hopping of any of the concerned particles or of the whole pair. Realistically, there must also be

additional dependencies on further neighbors, which are all neglected for simplicity.

Equilibrium states of DPLM are exactly solvable. In particular, particle occupancies n_i follow equilibrium statistics the same as those of a standard identical-particle lattice gas model with a constant interaction energy. These will be explained in Appendix A. Furthermore, equilibrium states of DPLM can be directly constructed using those of standard lattice gas, which exhibits no glassy slowdown (see Appendix B 5).

The dynamics of DPLM is defined by standard activated hopping approach for kinetic Monte Carlo simulations. Specifically, to simulate the dynamics at temperature T , each particle can hop to an unoccupied NN site at a rate²⁵

$$w = w_0 \exp\left(-\frac{E_0 + \Delta E/2}{k_B T}\right) \quad (5)$$

where ΔE is the change in the system energy due to the hop and $k_B = 1$ is the Boltzmann constant. This definition satisfies detailed balance. We let $E_0 = 1.5$ so that $E_0 + \Delta E/2 \geq 0$. Also, we put $w_0 = 10^6$ without loss of generality. Particle motions can be equivalently described as void motions (see Fig. 1). At temperature $T \rightarrow \infty$, DPLM reduces to a simple sliding block model²⁶.

III. GLASSY DYNAMICS

Let $\phi_v = 1 - \phi$ be the void density where $\phi = N/L^2$ is the particle density in principle related physically to the system pressure. We perform kinetic Monte Carlo simulations of fully equilibrated systems at $L = 100$ at various T and ϕ_v (see Appendix B for simulation methods). Standard dynamical measurements show that the system behaves as a simple liquid at high T and ϕ_v and a glass at low T and ϕ_v . As will be further explained, glassy behaviors are shown by the appearance of a plateau in the particle mean square displacement (MSD), a super-Arrhenius T dependence of the particle diffusion coefficient D , a stretched exponential form of the self-intermediate scattering function decaying towards zero at long time, a violation of the Stokes-Einstein relation, and typical time and T dependences of a four-point susceptibility. In particular, the convergence of the self-intermediate scattering function towards zero rather than a finite value at long time verifies that DPLM is a model of structural glass, as opposed to for example spin glass. For all T and ϕ_v studied, DPLM exhibits no sign of ideal glass transition. It also appears ergodic as supported, for example, by the divergence of the particle MSD and the vanishing of the self-intermediate scattering function at long time.

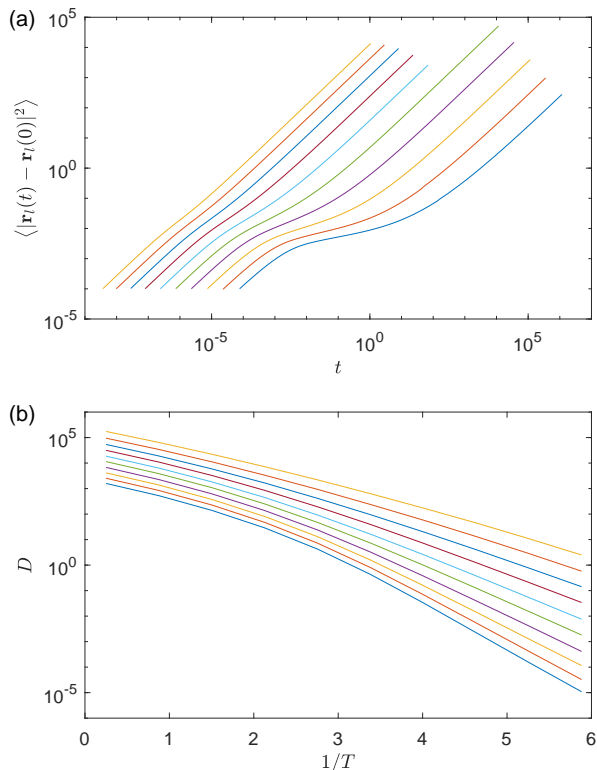


FIG. 2. (a) Particle mean square displacement (MSD) against t in log-log scale for $T = 0.170, 0.190, 0.216, 0.250, 0.296, 0.363, 0.470, 0.666, 1.142, 4.000$ and void density $\phi_v = 0.01$ with the highest T at the top. (b) Arrhenius plot of D for $\phi_v = 0.005, 0.008, 0.013, 0.021, 0.035, 0.056, 0.092, 0.149, 0.242, 0.392$, with the highest ϕ_v at the top.

A. Diffusion coefficient

We calculate the MSD defined as $\langle |\mathbf{r}_l(t) - \mathbf{r}_l(0)|^2 \rangle$ where $\mathbf{r}_l(t)$ denotes the lattice position vector of particle l at time t . Figure 2(a) shows the MSD in a log-log plot for different T and $\phi_v = 0.01$. For $t \rightarrow \infty$, the slopes of the lines are consistent with unity, indicating diffusive behavior over long observation time. Sub-diffusive plateaus appearing at intermediate t at low T indicate cage effects. Note that being a lattice model without vibrational modes at the sublattice level, the plateaus are much less pronounced as have been found for other lattice models¹⁰.

From similar MSD for various T and ϕ_v , we measure the particle diffusion coefficient

$$D = \frac{1}{2d} \lim_{t \rightarrow \infty} \frac{\langle |\mathbf{r}_l(t) - \mathbf{r}_l(0)|^2 \rangle}{t} \quad (6)$$

by fitting to data points where $\langle |\mathbf{r}_l(t) - \mathbf{r}_l(0)|^2 \rangle > 1$ and the slope in the log-log plot is higher than 0.96. Fig. 2(b) shows D in an Arrhenius plot for various ϕ_v . It exhibits super-Arrhenius behavior which becomes more pronounced at small ϕ_v and low T . This shows that DPLM is a fragile glass.

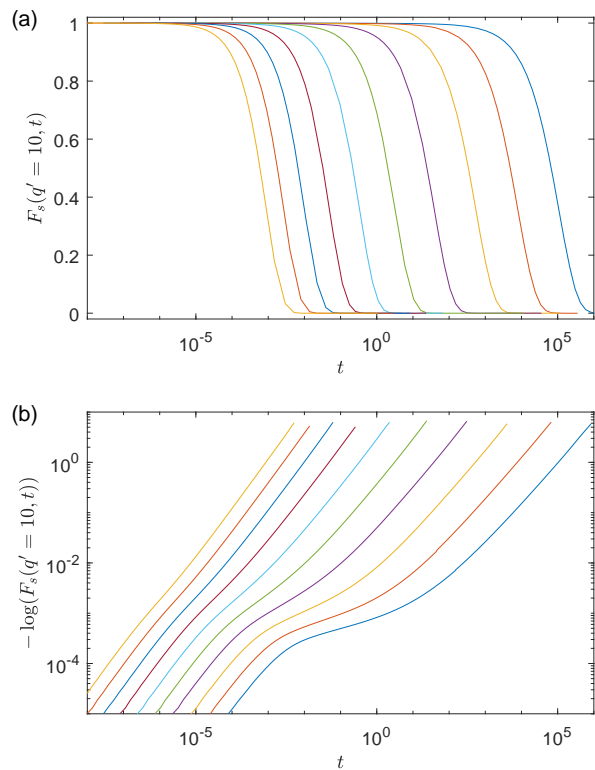


FIG. 3. (a) Decays of self-intermediate scattering function $F_s(q, t)$ in linear-log scale, for the same values of T used in Fig. 2(a), with T decreasing from left to right. Wavenumber $q = (2\pi/L)q' = \pi/5$ and $\phi_v = 0.01$ are used here. (b) Same data as in (a) in log-log-versus-log scale. Data corresponding to $F_s(q, t) < 10^{-3}$ are noisy and are omitted. The slope of the linear region at large t with $10^{-3} \leq F_s(q, t) \leq 0.9$ gives the stretching exponent β .

B. Self-intermediate scattering function

We have measured the self-intermediate scattering function defined as

$$F_s(\mathbf{q}, t) = \left\langle e^{i\mathbf{q} \cdot (\mathbf{r}_l(t) - \mathbf{r}_l(0))} \right\rangle \quad (7)$$

and the result is shown in Fig. 3(a) for $\phi_v = 0.01$ and $q = (2\pi/L)q'$ with $q' = 10$. A one-step drop of $F_s(q, t)$ versus t instead of a two-step decay is again typical for lattice models^{10,12,27}. In glassy systems, the terminal decay of the scattering function is usually well approximated by the Kohlrausch-Williams-Watts (KWW) stretched exponential function of the form $A \exp(-(t/\tau)^\beta)$, where τ is a relaxation time and β ($0 < \beta < 1$) is the stretching exponent. Our results fit well to the KWW form for large t . This is also demonstrated by the log-log plot of $-\log(F_s(q, t))$ against t in Fig. 3(b) which shows a linear region at large t expected from the KWW form with $A \simeq 1$. The stretching exponent obtained from the slope of the linear region is plotted in Fig. 4(a). As T decreases, β drops from 1 to around 0.82, indicating glassy dynamics at low T .

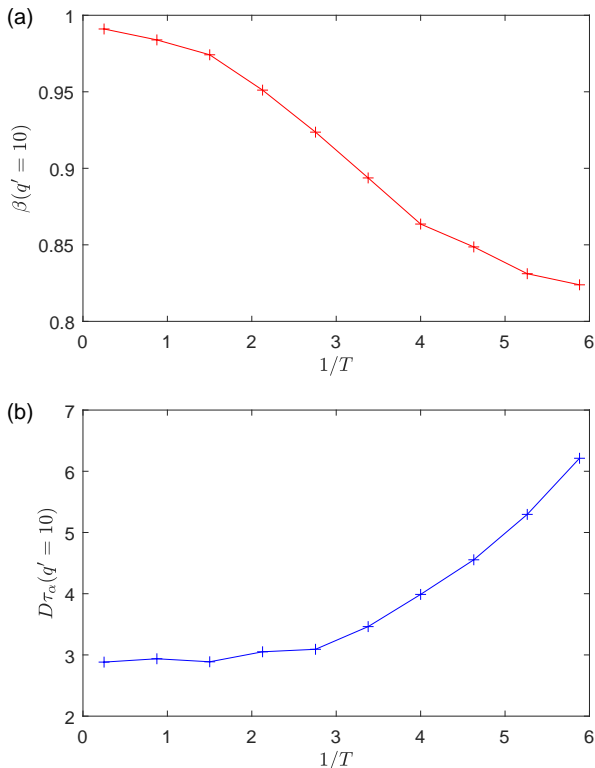


FIG. 4. (a) Stretching exponent β plotted against $1/T$ for $\phi_v = 0.01$. (b) Violation of the Stokes-Einstein relation, $D\tau_\alpha = \text{constant}$ where τ_α is a relaxation time.

From Fig. 3(a), we also extract a relaxation time τ_α which is the time at which $F_s(q, t) = 1/e$. Fig. 4(b) plots $D\tau_\alpha$ against $1/T$. The value clearly increases with decreasing T and demonstrate a violation of the Stokes-Einstein relation expected for glasses.

C. Four-point correlation function

Close to the glass transition, one region in a glassy fluid can relax much faster than another one. This spatially inhomogeneous dynamical behavior is known as dynamic heterogeneity. To quantitatively study the heterogeneity in the persistence of the particle configuration, one can define an overlap function as

$$c_l(t, 0) = e^{i\mathbf{q} \cdot (\mathbf{r}_l(t) - \mathbf{r}_l(0))}. \quad (8)$$

It measures how much particle l moves during times 0 and t at a length scale $2\pi/q$. Note that the average overlap equals the self-intermediate scattering function $F_s(\mathbf{q}, t)$. Each particle contributes to an overlap field defined by

$$c(\mathbf{r}; t, 0) = \sum_l c_l(t, 0) \delta(\mathbf{r} - \mathbf{r}_l(0)) \quad (9)$$

Consider its spatial correlation

$$G_4(\mathbf{r}, t) = \langle c(\mathbf{r}; t, 0)c(\mathbf{0}; t, 0) \rangle - \langle c(\mathbf{0}; t, 0) \rangle^2 \quad (10)$$

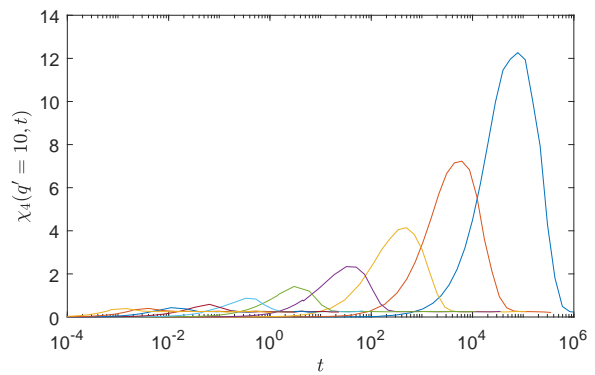


FIG. 5. $\chi_4(t)$ for $\phi_v = 0.01$ and the same values of T used in Fig. 2(a). T decreases from left to right.

where the average is over the spatial origin $\mathbf{0}$ and the starting time 0. G_4 measures the correlation of the fluctuations in the overlap function between two points that are separated by \mathbf{r} .

In the Fourier space, we get

$$S_4(\tilde{\mathbf{q}}, t) = \int e^{i\tilde{\mathbf{q}} \cdot \mathbf{r}} G_4(\mathbf{r}, t) d\mathbf{r} \quad (11)$$

$$= N \left\langle \left| \frac{1}{N} \sum_l e^{i\tilde{\mathbf{q}} \cdot \mathbf{r}_l(0)} (c_l(t, 0) - F_s(\mathbf{q}, t)) \right|^2 \right\rangle \quad (12)$$

One can define the susceptibility as $\chi_4(t) = \lim_{\tilde{q} \rightarrow 0} S_4(\tilde{\mathbf{q}}, t)$, which is simply the variance of the overlap function. $\chi_4(t)$ can be interpreted as the typical size of correlated clusters in structural relaxation, thus an efficient measure of the degree of dynamic heterogeneity.

Fig. 5 shows $\chi_4(t)$ from DPLM simulations. As is typical for structural glasses, for each temperature, $\chi_4(t)$ has a peak, which shifts to larger times, and has a larger value when T decreases. This reveals an increasing length scale of dynamic heterogeneity when the system cools down.

IV. EMERGENT FACILITATION BEHAVIORS

Being an energetically non-trivial model with T and ϕ_v independently and fully tunable, it exhibits much richer physics than purely kinetic models such as KCM. The particle diffusion coefficient D shown in Fig 2(b) is replotted in Fig. 6(a) against ϕ_v . At each T , the linear relation in the log-log plot at small ϕ_v suggests the power-law

$$D \sim \phi_v^\alpha. \quad (13)$$

Fig. 6(b) plots the scaling exponent α as a function of T . For the liquid state at high T , we get $\alpha \simeq 1$ indicating that each void moves independently²⁶. This is supported by a video in the Supplemental Material²⁸ showing the motions of the voids as well as the particles at $T = 0.5$.

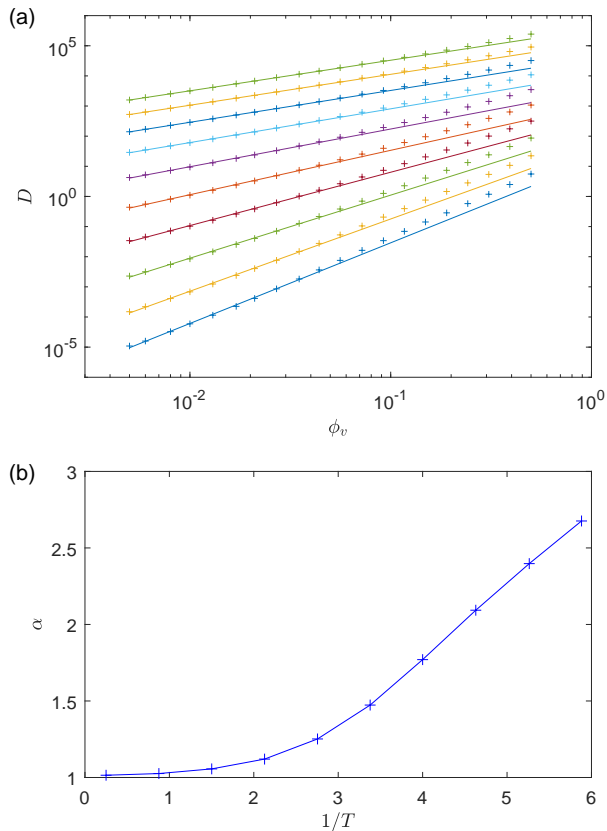


FIG. 6. (a) Particle diffusion coefficient D against void density ϕ_v in log-log scale for values of T used in Fig. 2(a) with the highest T at the top. (b) Scaling exponent α against $1/T$ obtained from linear fits to data in (a) with $\phi_v \leq 0.05$.

It can be observed that voids diffuse independently. Figure 7(a) visualizes the same motions using void trajectories (thin lines). They appear slightly more compact than those of simple random walks due to the disorder. Particles with non-zero net displacements (pink and red) induced by the same void can be grouped into a cluster. Cluster sizes for different voids are relatively uniform. Voids are not trapped and travel throughout the whole system independently at longer times. Dynamic heterogeneity revealed via these clusters is weak.

We now explain that the low T regime exhibits dynamic facilitation¹⁹. Fig. 6(b) shows that α rises to 2 and beyond at low T . The nonlinear scaling dictates that a void at small ϕ_v has arbitrarily small contributions to the dynamics. According to simple chemical kinetics, $\alpha \simeq 2$ corresponds to motion dominated by pairs of coupled voids. This quantitatively shows an emergent dynamic facilitation behavior of void motions. It is analogous to KCM and in particular the spin facilitation dynamics of the FA model⁸. We have checked that the nonlinear scaling in Eq. (13) is not due to any void aggregation and is robust upon tuning the void-void attraction by a shift of the probability distribution g on the energy scale.

To verify the above facilitation interpretation of

Eq. (13), we directly visualize the particle motions for $T = 0.16$ in a video in the Supplemental Material²⁸. It can be seen that isolated voids are trapped. In sharp contrast, a pair of voids nearby to each other moves vigorously. Figure 7(b) shows the void trajectories in the same simulation which become very compact with numerous dead-ends indicating confined motions of the voids due to enhanced disorder. The trajectory of each isolated void induces no or few displaced particles (pink and red) as most particles have not hopped or have returned to their original positions. In contrast, the pair of voids nearby to each other induces significantly more extensive intertwining trajectories and vigorous particle displacements. Such pairs dominate the dynamics for the $\alpha \simeq 2$ regime. At longer times, isolated voids typically remain trapped locally by the disorder unless visited and untrapped by other mobile pairs. Pairs of voids may split and new pairs may emerge but these occur at a longer time scale. Dynamic heterogeneity induced by highly mobile pairs of voids among trapped isolated voids is thus strong. Fig. 6(b) suggests that α may reach 3 and beyond at even lower T indicating dynamics dominated by triplets of voids, etc.

The dynamics of an isolated void at low T typically involve motions confined along low-energy paths. Note that n hops by a single void typically corresponds to n single-hops by n particles as shown in Fig. 1. A trapped void hence typically leads to bistable-like back-and-forth hops by a few particles. Such repetitive motions observed in MD simulations of polymers have been argued as the main cause of super-Arrhenius slow-down²⁹. We have adapted the method in Ref. 29 to quantify these repetitions. Specifically, after a particle has hopped, we measure the probability P_{ret} that its next hop returns itself to the original site. The probability P_2 that it next hops instead to a new site is also measured. The results for $\phi_v = 0.01$ are plotted in Fig. 8. They follow $P_{ret} + P_2 = 1$ within 0.01% and the minor deviations are due to particles without a second hop during the observed period. At large T , we find empirically that $P_{ret} \simeq 1/2$ applicable for small ϕ_v noting that the random walks of voids induce correlated walks of particles³⁰. We have checked that P_{ret} approaches towards the particle random walk value $1/4$ at large ϕ_v . As T decreases, P_{ret} increases monotonically reaching 0.96 for the lowest T studied. The trend strikingly resembles those from polymer simulations²⁹. This resemblance also strongly supports the physical relevance of DPLM. Such a high P_{ret} means that most hops are reversed and irrelevant to long-time dynamics. The repetition thus must contribute significantly to the slowdown. As $T \rightarrow 0$, our results support $P_{ret} \rightarrow 1$. Most hopping particles then form two-level systems (TLS) known to be relevant to glass at very low T ³¹.

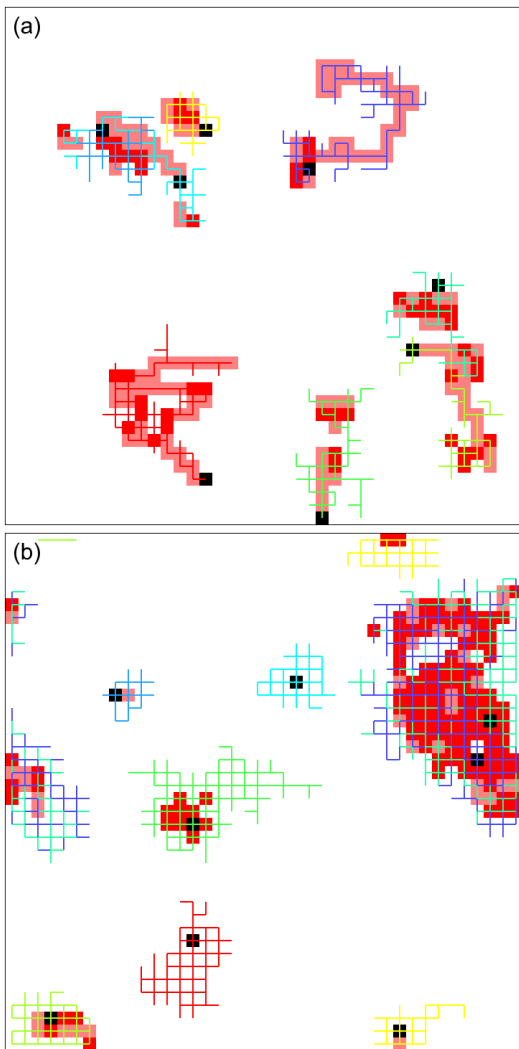


FIG. 7. (a) A snapshot from a small-scale simulation on a 40×40 lattice with 1592 particles and 8 voids, i.e. $\phi_v = 0.005$. It shows the final positions of voids (black squares) after a short simulation duration of $\Delta\tau = 10^{-3}$ at $T = 0.5$. Particles with net displacements 0, 1, and > 1 during the period are shaded in white, pink and red respectively. Each thin line shows the trajectory of a void and is colored randomly. (b) Similar to (a) with $T = 0.16$ and $\Delta\tau = 5 \times 10^4$. In both (a) and (b), the particle MSD during the period is about 0.5. Particle dynamics are shown in videos in the Supplemental Material²⁸.

V. CONCLUSION

We have developed DPLM as a lattice gas model based on distinguishable particles for studying glassy dynamics. In the glassy phase, the particle diffusion coefficient scales nonlinearly with the void density in the low void density limit. This implies that isolated voids are essentially trapped and the dynamics of a void is dominated by facilitation by other voids nearby. Particle hopping becomes increasingly repetitive at low temperature.

DPLM is defined by a simple, generic, and physically

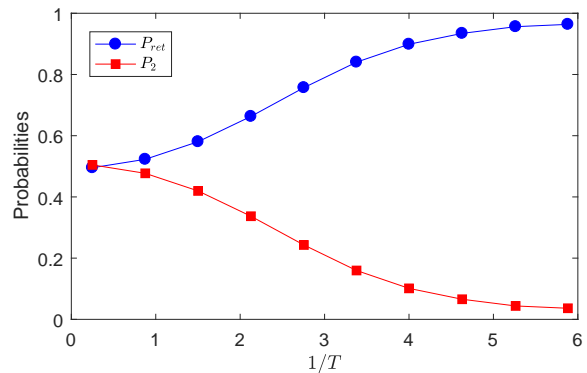


FIG. 8. Probabilities P_{ret} and P_2 for returning and non-returning second hops against $1/T$ for $\phi_v = 0.01$.

motivated system energy function. It has both non-trivial energetics and kinetics. It can be efficiently simulated and equilibrium states can be directly generated at arbitrary temperature and density. Its glassy state does not rely on frustration on a specific lattice type. These may render DPLM a unique prototypical model for the further study of glassy dynamics and aging in disordered systems.

The definition of DPLM involves no explicit facilitation rule but facilitation behaviors are observed. It thus provides a strong microscopic support to dynamic facilitation and KCM. It will be interesting to deduce the precise coarse-grained lattice model for DPLM. Dynamic facilitation of voids demonstrated by DPLM is analogous to the picture of facilitation via pair-interactions of string-like particle motions motivated by MD simulations of polymers²⁹. In that picture, each string is initiated by a single void leading to a one-one correspondence between strings and voids. From Fig. 1, the motion of a void alters the particle pairings and hence the energy landscape along its entire path. The energy landscape experienced by another void nearby is thus altered. Whether the second void can diffuse across the path of the first void is thus randomly affected. This demonstrates a form of path interaction of voids which is essentially equivalent to string interactions observed in MD²⁹. The particle and void dynamics in DPLM as well as in polymer simulations is recently described on the same footing by a random local configuration tree theory³². Alternatively, it will also be of interest to study DPLM defined on the Bethe lattice which may allow exact analysis.

In DPLM, each V_{ijkl} is an independent random variable. More generally, Eq. (2) features a very generic Hamiltonian. Adopting instead a constant $V_{ijkl} \equiv V$ gives a simple interacting lattice gas. As lattice gas models can be mapped to spin models with spin-exchange (Kawasaki) dynamics, it also represents a ferromagnetic or anti-ferromagnetic spin model. Alternatively, a particle-dependent $V_{ijkl} \equiv V_{kl}$ reduces it to a multi-species lattice gas such as a binary alloy³³. Limiting

to a site-dependent $V_{ijkl} \equiv V_{ij}$, it becomes a variant of the Edwards-Anderson (EA) model for spin glass⁶ with Kawasaki dynamics and a random field. In addition, by continuously varying the correlations between the various V_{ijkl} , Eq. (2) describes models interpolating between these systems.

ACKNOWLEDGMENTS

We thank helpful discussions with J.Q. You, Ho-Kei Chan and Peter Harrowell. We are grateful to the support of Hong Kong GRF (Grant 15301014).

Appendix A: Exact equilibrium statistics

Assuming ergodicity, which is supported by our simulations in Sec. III, it is possible to derive exact equilibrium states of DPLM in the thermodynamic limit. This is because the system follows a Boltzmann distribution which factorizes over the bonds. More specifically, equilibrium statistics in the ergodic phase of a system with N particles is described by the canonical partition function

$$Z = \sum_{\{s_i\}} e^{-\beta E} \quad (\text{A1})$$

where the sum is over all possible system states $\{s_i\}$ and $\beta = 1/k_B T$. Noting that $s_i = 0$ denotes a void, Z can be rewritten as

$$Z = \sum_{\{n_i\}} \sum_{\{s_i > 0\} \in \mathcal{P}_N} e^{-\beta E}. \quad (\text{A2})$$

Here, the first sum is over all possible site occupancies $\{n_i\}$ with n_i defined in Eq. (1). The second sum is over the set \mathcal{P}_N of the $N!$ permutations of particle arrangement $\{s_i > 0\}$ at the N occupied sites with $n_i = 1$. Equation (A2) can be recast into

$$Z = \sum_{\{n_i\}} Z_{\{n_i\}} \quad (\text{A3})$$

where $Z_{\{n_i\}}$ is the partition function restricted to the specific site occupation $\{n_i\}$ and is given by

$$Z_{\{n_i\}} = \sum_{\{s_i > 0\} \in \mathcal{P}_N} \prod_{\langle ij \rangle'} e^{-\beta V_{ij s_i s_j}}. \quad (\text{A4})$$

after applying Eq. (3).

1. Quenched and annealed averaging

The value of primary interest is the quenched average $\overline{\ln Z}$ where the bar denotes averaging over the time-independent variables V_{ijkl} . At sufficiently high T , it may agree with the annealed average $\ln \langle Z \rangle_a$, where $\langle \cdot \rangle_a$ again

denotes averaging over V_{ijkl} which is now reinterpreted as additional time-dependent system state variables. A detailed derivation of this agreement will be explained in Appendix A 2.

We first study annealed averages which are much easier to calculate. Applying annealed averaging to Eq. (A4), we get

$$\langle Z_{\{n_i\}} \rangle_a = \sum_{\{s_i > 0\} \in \mathcal{P}_N} \prod_{\langle ij \rangle'} \langle e^{-\beta V_{ij s_i s_j}} \rangle_a \quad (\text{A5})$$

where we have noted that each $V_{ij s_i s_j}$ has a distinct set of indices and are thus independent random numbers. Defining

$$e^{-\beta U} = \langle e^{-\beta V_{ij s_i s_j}} \rangle_a, \quad (\text{A6})$$

U can then be interpreted as the average free energy of a bond between two NN particles and is given by

$$U = -\frac{1}{\beta} \ln \int_{-\infty}^{\infty} e^{-\beta V} g(V) dV. \quad (\text{A7})$$

Substituting Eq. (A6) into Eq. (A5), all terms in the sum become identical and this trivially gives

$$\langle Z_{\{n_i\}} \rangle_a = N! \prod_{\langle ij \rangle'} e^{-\beta U}. \quad (\text{A8})$$

It further reduces to

$$\langle Z_{\{n_i\}} \rangle_a = N! e^{-\beta N_b U} \quad (\text{A9})$$

where N_b is the number of pairs of bonded particles for the given site occupation $\{n_i\}$. Substituting into the annealed average of Eq. (A3), we get

$$\langle Z \rangle_a = N! \sum_{\{n_i\}} e^{-\beta N_b U} \quad (\text{A10})$$

The factor $N!$ results from the particle distinguishability and is related to the Gibb's paradox³⁴. It is irrelevant and can be omitted for canonical ensembles with a constant N considered here. We thus redefine Z by multiplying with a factor $1/N!$ and obtain

$$\langle Z \rangle_a = \sum_{\{n_i\}} e^{-\beta N_b U}. \quad (\text{A11})$$

2. Averaging over permutations

As discussed above, it is valid to redefine Z with an additional factor $1/N!$. Specifically, we continue to adopt Eq. (A3) while Eq. (A4) is replaced by

$$Z_{\{n_i\}} = \frac{1}{N!} \sum_{\{s_i > 0\} \in \mathcal{P}_N} \prod_{\langle ij \rangle'} e^{-\beta V_{ij s_i s_j}}. \quad (\text{A12})$$

The r.h.s. now involves explicitly an average over particle permutations among the occupied sites. We will now

explain that this averages out all $V_{ij s_i s_j}$. This is because as emphasized in Eq. (4), $V_{ij s_i s_j}$ with nontrivial indices s_i and s_j is not quenched. It indeed samples over many different V_{ijkl} as particles permute, in sharp contrast to the quenched V_{ijkl} at fixed indices.

Without loss of generality, assume that sites 1 and 2 are occupied nearest neighboring sites. We single out the permutations concerning sites 1 and 2, giving

$$Z_{\{n_i\}} = \frac{1}{N(N-1)} \sum_{\substack{s_1, s_2=1 \\ s_1 \neq s_2}}^N e^{-\beta V_{12 s_1 s_2}} Z_{N-2}(s_1, s_2) \quad (\text{A13})$$

where $Z_{N-2}(s_1, s_2)$ is the partition function for the remain $N-2$ sites excluding particles s_1 and s_2 defined as

$$Z_{N-2}(s_1, s_2) = \frac{1}{(N-2)!} \times \sum_{\substack{\{s_i > 0\} \in \mathcal{P}_{N-2} \\ s_i \neq s_1, s_2}} \prod_{\substack{\langle ij \rangle' \\ \{i, j\} \neq \{1, 2\}}} e^{-\beta V_{ij s_i s_j}}. \quad (\text{A14})$$

Since all particles are statistically equivalent, the dependence of $Z_{N-2}(s_1, s_2)$ on s_1 and s_2 is a manifestation of random fluctuations resulting from the random V_{ijkl} . Assuming negligible fluctuations in $Z_{N-2}(s_1, s_2)$ at large N , which will be justified later, we write $Z_{N-2} \equiv Z_{N-2}(s_1, s_2)$ and Eq. (A13) reduces to

$$Z_{\{n_i\}} = e^{-\beta U} Z_{N-2} \quad (\text{A15})$$

where U is defined in Eq. (A7). Repeating similar procedures, a factor $e^{-\beta U}$ is contributed by every bond and we get

$$Z_{\{n_i\}} = e^{-\beta N_b U} \quad (\text{A16})$$

analogous to Eq. (A9) after irrelevant prefactors in the latter are dropped.

At finite N , $Z_{\{n_i\}}$ for a given set of V_{ijkl} deviates from the value in Eq. (A16) with a magnitude characterized by the standard deviation σ_Z . We will show that σ_Z becomes negligible compared with $Z_{\{n_i\}}$ as N increases. At high T , this is obvious because fluctuations of each factor $e^{-\beta V_{ij s_i s_j}}$ in Eq. (A12) is small. We thus focus only on the case of low T . The deduction is non-trivial because terms in Eq. (A12) are correlated and have large variances increasing with N .

At low T , a term in Eq. (A12) is significant predominantly when all its factors are relatively large. We thus characterize each factor only by whether it is large or small via the approximation

$$e^{-\beta V_{ij s_i s_j}} \simeq \frac{\xi_{ij}}{2k_B T} e^{-\beta U} \quad (\text{A17})$$

where

$$\xi_{ij} = \begin{cases} 1 & \text{for } V_{ij s_i s_j} \in [V_0, V_0 + 2k_B T] \\ 0 & \text{otherwise} \end{cases} \quad (\text{A18})$$

with $V_0 = -0.5$. Noting that the apriori probability density $g(V_{ij s_i s_j})$ of $V_{ij s_i s_j}$ is uniform in $[V_0, V_0 + 1]$, we have constructed the approximation so that the average $e^{-\beta U}$ of $e^{-\beta V_{ij s_i s_j}}$ is unchanged. In particular, the probability p that $\xi_{ij} = 1$ is

$$p = 2k_B T. \quad (\text{A19})$$

Equation (A12) is then approximated by

$$Z_{\{n_i\}} \simeq \frac{1}{N!} p^{-N_b} e^{-\beta N_b U} M \quad (\text{A20})$$

where

$$M = \sum_{\{s_i > 0\} \in \mathcal{P}_N} \prod_{\langle ij \rangle'} \xi_{ij}. \quad (\text{A21})$$

Here, M equals the number of relevant particle permutations which contribute significantly to $Z_{\{n_i\}}$. For each of these permutations, it is easy to see that all interactions are within $k_B T$ from the average value $V_0 + k_B T$.

We now evaluate the statistical properties of M by tackling the combinatorial problem of counting the relevant permutations. For simplicity, we illustrate further calculations for a fully occupied $N \times 1$ lattice with interactions only in the non-trivial dimension, but generalization is straightforward. First, there are N ways to occupy site 1. For each choice, there are on average $(N-1)p$ ways to occupy site 2 in which $\xi_{12} = 1$. It is analogous for the other sites except for $i = N$ which contributes a factor p^2 because both $\xi_{N-1, N}$ and ξ_{1N} must be nonzero. The average of M is thus

$$\begin{aligned} \bar{M} &= N \cdot (N-1)p \cdot (N-2)p \cdots 1p^2 \\ &= N! p^N \end{aligned} \quad (\text{A22})$$

As a consistency check, substituting Eq. (A22) into Eq. (A20) and assuming $M \simeq \bar{M}$ recovers Eq. (A16).

More importantly, we now calculate the standard deviation σ_M of M . For each of the N ways to occupy site 1, the number of ways to occupy site 2 follows a binomial distribution with a variance $(N-1)p(1-p)$. Each of these choices at sites 1 and 2 on average results at $(N-2)!p^{N-1}$ relevant ways to permute the remaining $N-2$ particles. Therefore, fluctuations at $i = 2$ contribute a variance v_2 to M given by

$$\begin{aligned} v_2 &= N \times (N-1)p(1-p) \times [(N-2)!p^{N-1}]^2 \\ &= \frac{(1-p)\bar{M}^2}{N(N-1)p} \end{aligned} \quad (\text{A23})$$

where we have used Eq. (A22). We next consider fluctuation at site 3 as a further example. For each of the on average $N(N-1)p$ ways to occupy sites 1 and 2, the number of ways to occupy site 3 follows a binomial distribution with a variance $(N-2)p(1-p)$. Each of these choices at sites 1, 2 and 3 on average results at $(N-3)!p^{N-2}$ relevant ways to permute the remaining

$N - 3$ particles. Fluctuations at site 3 thus contribute a variance v_3 to M given by

$$\begin{aligned} v_3 &= N(N-1)p \times (N-2)p(1-p) \times [(N-3)!p^{N-2}]^2 \\ &= \frac{(1-p)\bar{M}^2}{N(N-1)(N-2)p^2} \end{aligned} \quad (\text{A24})$$

Fluctuations at other sites can be similarly calculated. Neglecting correlations between these fluctuations, we get $\sigma_M^2 = \sum_{i=2}^N v_i$ which simplifies to

$$\begin{aligned} \sigma_M^2 &= (1-p)\bar{M}^2 \left(\frac{1}{N(N-1)p} + \frac{1}{N(N-1)(N-2)p^2} \right. \\ &\quad \left. + \frac{1}{N(N-1)(N-2)(N-3)p^3} + \dots \right) \end{aligned} \quad (\text{A25})$$

For large N , all but the first term are negligible and we get $\sigma_M \simeq \sqrt{(1-p)/p} \bar{M}/N$. Since $Z_{\{n_i\}} \propto M$ according to Eq. (A20), the standard deviation of $Z_{\{n_i\}}$ is $\sigma_Z \simeq \sqrt{(1-p)/p} Z_{\{n_i\}}/N$. In particular, we have

$$\sigma_Z \sim \frac{Z_{\{n_i\}}}{N} \quad (\text{A26})$$

To verify this result, we have numerically performed direct enumeration of 10^5 values of $Z_{\{n_i\}}$ using either Eq. (A12) or Eq. (A20) for 10^5 independent realizations of V_{ijkl} for $N \leq 11$ and $T \geq 0.2$. In both cases, Eq. (A26) is readily verified. As a further check of our method, we consider alternative interactions in the form $V_{ijkl} \equiv V_{kl}$, representing particle-dependent interactions as opposed to site-particle-dependent ones. Using analogous arguments, we find instead $\sigma_Z \sim Z_{\{n_i\}}$, which is also well verified numerically by direct enumeration.

It is straightforward to generalize Eq. (A26) to arbitrary site occupancies n_i in 2D. Therefore, for DPLM studied in this work, Eq. (A16) admits corrections only of order $1/N$ and is essentially exact for large N . Substituting Eq. (A16) into Eq. (A3), we get

$$Z = \sum_{\{n_i\}} e^{-\beta N_b U} \quad (\text{A27})$$

where all V_{ijkl} -dependent correction terms are of higher orders in $1/N$. Note that similar arguments also imply that $Z_{N-2}(s_1, s_2)$ defined in Eq. (A14) has negligible fluctuations and this justifies the assumption used in deriving Eq. (A15).

We emphasize that we have *not* at this point performed the ensemble average over V_{ijkl} and Z in Eq. (A27) have already become independent of V_{ijkl} due to the averaging over particle permutations. This is quite analogous to self-averaging behaviors exhibited by many systems. Here, sample to sample fluctuations of Z hence vanish and all quenched averaging becomes trivial, i.e. $\overline{\ln Z} = \ln Z$. A further comparison of Eq. (A27) with Eq. (A11) gives

$$\overline{\ln Z} = \ln Z = \ln \langle Z \rangle_a. \quad (\text{A28})$$

This shows the identical statistical properties of quenched and annealed ensembles in the ergodic phase for large N .

3. Equilibrium properties

Let Z_{LG} be the partition function of a simple identical-particle lattice gas with a NN particle interaction energy U . It is easy to see that Z_{LG} is in fact identical to Z in Eq. (A27), i.e.

$$Z = Z_{LG}. \quad (\text{A29})$$

Therefore, DPLM and simple lattice gas have exactly the same equilibrium particle occupation statistics despite the very different dynamics. A simple lattice gas has a gas-liquid phase transition at the vaporization temperature T_v , which depends on U and thus on the distribution g . The lattice gas can be further mapped to the 2D Ising model with an exchange $J = -U/4$ ³³. Applying Onsager's solution $T_v = 2J/\ln(1 + \sqrt{2})$ for the 2D Ising model³⁴, we get

$$T_v = \frac{-U}{4 \ln(1 + \sqrt{2})} \quad (\text{A30})$$

where U is given in Eq. (A7) evaluated at $T = T_v$. Solving Eqs. (A7) and (A30) numerically, we get $T_v \simeq 0.132$. We have verified this value of T_v using small-scale DPLM simulations at e.g. $\phi_v = 0.5$. Since T_v is below T studied in our main simulations, the systems considered here correspond to lattice gases in the gaseous phase, in which particles are only slightly attractive and neither particles nor voids in dilute concentration aggregate.

We now derive the equilibrium distribution of the interactions for annealed ensembles, which is identical to that of quenched ensembles according to Eq. (A28). Restricting our consideration to a given site occupancy $\{n_i\}$. We study the equilibrium properties of the remaining state variables $s_i > 0$ and V_{ijkl} . They follow the Boltzmann probability distribution

$$P_{eq}(\{s_i\}, \{V_{ijkl}\}) \propto e^{-\beta E} \prod_{\langle i,j \rangle, k,l} g(V_{ijkl}) \quad (\text{A31})$$

where the product is over all NN sites i and j and all particles k and l . Applying Eq. (3), we get

$$\begin{aligned} P_{eq}(\{s_i\}, \{V_{ijkl}\}) &\propto \left[\prod_{\langle i,j \rangle'} e^{-\beta V_{ijs_i s_j}} g(V_{ijs_i s_j}) \right] \\ &\times \left[\prod_{\{\langle i,j \rangle, k,l \} \in C} g(V_{ijkl}) \right] \end{aligned} \quad (\text{A32})$$

Here, the first product is restricted to bonded NN sites i and j . Thus, the realized interaction $V_{ijs_i s_j}$ which describes an existing bond in the state $\{s_i\}$ follows the Boltzmann distribution

$$p_{eq}(V_{ijs_i s_j}) = \frac{1}{\mathcal{N}} e^{-\beta V_{ijs_i s_j}} g(V_{ijs_i s_j}) \quad (\text{A33})$$

where $\mathcal{N} = \int e^{-\beta V} g(V) dV$ is a normalization constant. The second product in Eq. (A32) is over the complementary set C of unrealized interactions V_{ijkl} which do not

represent any existing bond in the state $\{s_i\}$. This equation also implies that these unrealized interactions simply follow $g(V_{ijkl})$.

We now further derive some other useful results. Adopting annealed ensemble, all s_i in the r.h.s. of Eq. (A32) are dummy indices of identical independent variables. All permutations of s_i are indeed equivalent and only amount to different labeling of the particles. To see this mathematically, we note that after integrating $P_{eq}(\{s_i\}, \{V_{ijkl}\})$ over all V_{ijkl} , we get a uniform probability distribution

$$P_{eq}(\{s_i\}) = 1/N! \quad (\text{A34})$$

demonstrating the equivalence of all $N!$ permutations $\{s_i\}$ for annealed ensembles as expected.

In addition, the average interaction between bonded particles is

$$\langle V_{ijs_iss_j} \rangle = \int V p_{eq}(V) dV \quad (\text{A35})$$

where p_{eq} is given in Eq. (A33). Using Eq. (3), the average energy per particle is then $\langle E \rangle / N = \langle N_b / N \rangle \langle V_{ijs_iss_j} \rangle$. For small ϕ_v with mostly isolated voids, the average number of bonds per particle is $\langle N_b / N \rangle \simeq 2(1 - \phi_v)$. This gives

$$\frac{\langle E \rangle}{N} = 2(1 - \phi_v) \int V p_{eq}(V) dV. \quad (\text{A36})$$

Appendix B: Simulation details

We will describe both elementary and accelerated simulation approaches, which have been checked to generate statistically identical results. Our main simulations are all performed using accelerated algorithms. Each of them at lattice size $L = 100$ takes up to about 20 hours to run on an Intel Xeon processor core. Data for each set of values of T and ϕ_v are typically averaged over 5 similar independent runs. Additional shorter runs recording particle positions at a higher time-resolution are also needed to obtain correlation data at short time.

1. Elementary kinetic Monte Carlo method

Simulations can be performed using standard kinetic Monte Carlo approach. At each time step Δt , the following procedures can be performed:

- Randomly choose a site i .
- Randomly choose a site j which is a NN of i .
- If $n_i = 1$ and $n_j = 0$ is false, reject this step.
- Accept particle hop from i to j with probability $4L^2 w \Delta t$ where w is calculated using Eq. (5)

Here, Δt must be small and satisfies $4L^2 w \Delta t \leq 1$ for all possible configurations.

2. Rejection-free method

The simple kinetic Monte Carlo algorithm above is inefficient due to too many rejected move attempts. A rejection-free method³⁵ is much more efficient. Let $N_v = L^2 - N$ be the number of voids. We optimize our algorithm for $\phi_v \simeq 0$ which is most demanding due to the slow dynamics. The number of possible hops is $4N_v$ in general. The associated hopping rates w are calculated using Eq. (5) and stored at the lowest level of a complete binary tree. Each parent node then stores the sum of the two immediate children. Note that an exchange of two voids is unphysical and is assigned a rate 0.

For each time step Δt , one of the $4N_v$ possible hops is randomly selected with a relative probability w . It is straightforward to select the hop efficiently by randomly descending the binary tree using the node values as the relative probabilistic weights. The hop is then executed. A few hopping rates associated with the hopping particle and its neighbors are recalculated since the local configuration has changed. The binary tree is then also updated accordingly. It is easy to see that Δt is time dependent and follows $\Delta t = 1/w_{root}$, where w_{root} is the value at the root of the binary tree and equals the sum of all the $4N_v$ rates³⁶.

3. Two-step interaction energy tabulation

A nontrivial point in the programming for DPLM is that the total number of V_{ijkl} is of order $N^2 L^2 \sim N^3$. This requires too much memory storage for large N . For medium values of N , V_{ijkl} can be sampled only when needed and stored using a hash data structure. In our main simulations with a large $N \sim L^2 = 10^4$, it is necessary to adopt a two-step tabulation method to be explained below.

As an approximate scheme, we put

$$V_{ijkl} = v(Q_i(k), Q_j(l)). \quad (\text{B1})$$

Here, each Q_i for site i is an independent random permutation function mapping the set $1, 2, \dots, N$ to itself. The function v thus involves only order N^2 tabulated random numbers sampled from g which are independent from each other except when the symmetry $v(k, l) = v(l, k)$ applies. Before simulation starts, the functions v and Q_i are randomly sampled and stored. The memory requirement significantly decreases from order N^3 to order N^2 . The method do introduce some unwanted correlations between the ideally independent V_{ijkl} . However, we have checked in medium scale simulations that it gives results statistically identical to those using the hash-table method.

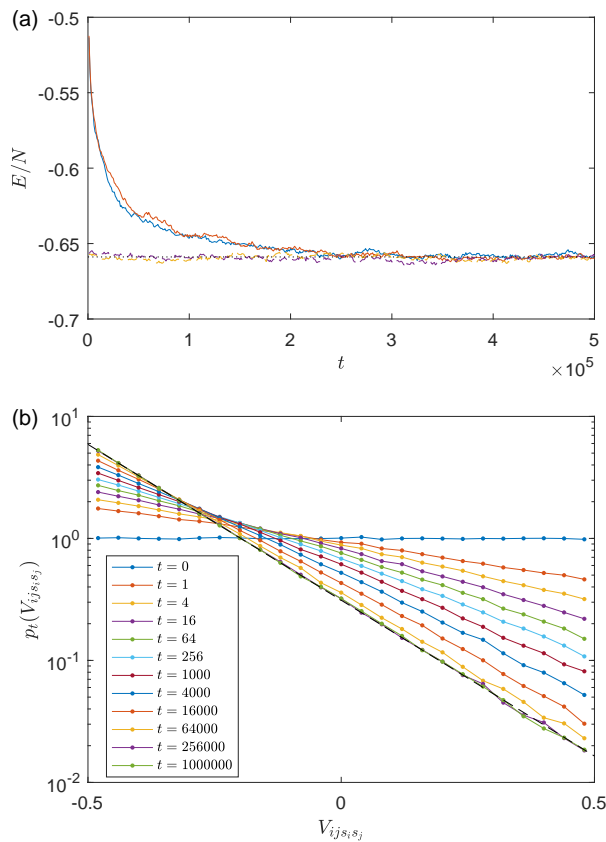


FIG. 9. (a) Plot of energy per particle E/N against time t from four independent runs adopting elementary (solid curves) and direct (dashed curves) initialization algorithms. The black dotted line shows $\langle E \rangle / N$ from Eq. (A36). (b) A semi-log plot of the probability distribution $p_t(V_{ij s_i s_j})$ of realized interaction $V_{ij s_i s_j}$ at time t from simulations adopting the elementary initialization algorithm. $p_t(V_{ij s_i s_j})$ for $t \geq 256000$ has converged to p_{eq} from Eq. (A33) indicated by the black dashed line. For both (a) and (b), $T = 0.170$ and $\phi_v = 0.01$.

4. Elementary initial thermalization

A straightforward approach is to generate each V_{ijkl} independently from the probability distribution g taking into account the symmetry $V_{ijkl} = V_{jilk}$. The system state is initialized at infinite temperature by putting each particle randomly onto an unoccupied site in the $L \times L$ lattice with uniform probability. This gives n_i and s_i at time $t = 0$. Thermalization kinetic Monte Carlo steps, typically performed using the rejection-free method explained above, are then conducted at the target temperature T until equilibrium is attained.

During thermalization, equilibrium is indicated by the stabilization of various statistical measures such as the average particle energy E/N . We have checked numerically that equilibration can be performed successfully under various conditions and a particularly demanding example in the glassy phase is illustrated in Fig. 9(a).

The solid curves show E/N against t from two typical runs for $T = 0.17$ and $\phi_v = 0.01$. They stabilize towards the average equilibrium value $\langle E \rangle / N$ given in Eq. (A36). Figure 9(b) shows the evolution of the probability distribution $p_t(V_{ij s_i s_j})$ of the realized interaction $V_{ij s_i s_j}$ at time t from the same runs. It crossovers smoothly from the initial distribution g toward the equilibrium distribution p_{eq} in Eq. (A33). From both Figs. 9(a) and (b), the system can be deemed equilibrium for the given T and ϕ_v for $t \gtrsim 2.5 \times 10^5$. The results verify numerically Eq. (A36) and Eq. (A33). More importantly, they hence also verify the agreement between quenched and annealed averages used in their derivations.

5. Direct initialization method

System equilibration at large N using thermalization Monte Carlo steps explained above can take very long runtime at low T . This is a major difficulty for many lattice models and most MD simulations of glass. Being able to directly construct equilibrium states is thus a highly desirable property. This is possible for KCM with trivial energetics, non-spatial models^{37,38} and some frustrated spin models defined on triangular or related lattices³⁹. It is also possible for MD simulations of a system with long-range shifted interactions^{23,24}. DPLM is in our knowledge the only finite-dimensional and energetically non-trivial lattice model of glass defined on a general lattice with this capability.

First, we calculate the particle occupancy n_i and the particle index s_i at every site i . We start by simulating a simple identical-particle lattice gas because of the equivalent particle statistics (see Eq. (A29)). It is performed with a constant NN particle interaction energy U given in Eq. (A7) and we use the same computer code for DPLM with V_{ijkl} reduced to the constant U . Similar to the elementary initial thermalization approach described above, we initialize the particle positions randomly and then equilibrate the simple lattice gas by a thermalization run. It is computationally very efficient because of the absence of glassification at arbitrary T . The thermalized particle positions give s_i and n_i at time $t = 0$. Note that due to the identical-particle nature of this part of the simulation, only n_i is of interest. The precise particle permutation as specified by s_i for the occupied sites is irrelevant because all permutations are equally probable (see Eq. (A34)).

Second, we randomly generate V_{ijkl} from the annealed ensemble, which is statistically identical to the quenched ensemble (see Eq. (A28)). Specifically, We sample all unrealized V_{ijkl} from the distribution g while realized interactions $V_{ij s_i s_j}$ appearing in the state $\{s_i\}$ are sampled from the Boltzmann distribution p_{eq} given by Eq. (A33). This completes the generation of an equilibrium state at T .

In Fig. 9(a), the two dashed curves show the particle energy E/N from two typical runs using this direct ini-

tialization method. They support that the systems have attained equilibrium energy once constructed and this numerically verifies the method. Note that at finite N , interactions from this approach differ in principle from that based on the elementary method in Appendix B 4 in which all interactions are sampled from g . Nevertheless, since the total number of V_{ijkl} is of order N^3 while the number of bonds is of order N , the fraction of realized interactions sampled from p_{eq} is only of order $1/N^2$. The fraction thus approaches zero at large N and this demonstrates the equivalence of the elementary and the direct methods. Even after using our two-step tabulation approximation in Eq. (B1), the fraction increases to order $1/N$ and still vanishes for large N . This approach of determining the particle arrangement n_i and s_i before generating the interaction V_{ijkl} is closely analogous to a planting method in Refs. 23 and 24.

6. Software reliability

Correct software implementation is highly nontrivial because minor programming mistakes may affect the particle dynamics only occasionally and can be very difficult to spot. One helpful consistency check is to measure the probability distribution of the interaction energy $V_{ijs_i s_j}$ at equilibrium and compare with the exact distribution in Eq. (A33). We have also conducted more general Boltzmann distribution tests³⁶ by performing long simulations using a small lattice with all but several particles frozen. Then, only a few thousand different configurations will be realized. We measure the total occurrence durations and the system energies of all these configurations and make sure that the results agree with the Boltzmann distribution within the expected statistical errors. With these tests, we believe that our software implementation is highly reliable.

-
- * Present address: Department of Physics, Carnegie Mellon University, Pittsburgh, Pennsylvania 15213
 † Email: C.H.Lam@polyu.edu.hk
- ¹ G. Biroli and J. P. Garrahan, *J. Chem. Phys.* **138**, 12A301 (2013)
 - ² F. H. Stillinger and P. G. Debenedetti, *Annu. Rev. Condens. Matter Phys.* **4**, 263 (2013)
 - ³ L. Berthier and G. Biroli, *Rev. Mod. Phys.* **83**, 587 (2011)
 - ⁴ W. Kob and H. C. Andersen, *Phys. Rev. E* **51**, 4626 (1995)
 - ⁵ K. Kremer and G. S. Grest, *J. Chem. Phys.* **92**, 5057 (1990)
 - ⁶ S. F. Edwards and P. W. Anderson, *Journal of Physics F: Metal Physics* **5**, 965 (1975)
 - ⁷ T. R. Kirkpatrick and D. Thirumalai, *Phys. Rev. B* **36**, 5388 (1987)
 - ⁸ G. H. Fredrickson and H. C. Andersen, *Phys. Rev. Lett.* **53**, 1244 (1984)
 - ⁹ R. G. Palmer, D. L. Stein, E. Abrahams, and P. W. Anderson, *Phys. Rev. Lett.* **53**, 958 (1984)
 - ¹⁰ W. Kob and H. C. Andersen, *Phys. Rev. E* **48**, 4364 (1993)
 - ¹¹ G. Biroli and M. Mézard, *Phys. Rev. Lett.* **88**, 025501 (2001)
 - ¹² R. K. Darst, D. R. Reichman, and G. Biroli, *J. Chem. Phys.* **132**, 044510 (2010)
 - ¹³ N. B. Tito, J. E. Lipson, and S. T. Milner, *Soft Matter* **9**, 3173 (2013)
 - ¹⁴ T. R. Kirkpatrick, D. Thirumalai, and P. G. Wolynes, *Phys. Rev. A* **40**, 1045 (1989)
 - ¹⁵ T. R. Kirkpatrick and D. Thirumalai, *Rev. Mod. Phys.* **87**, 183 (2015)
 - ¹⁶ T. Kirkpatrick and D. Thirumalai, *J. Phys. A* **22**, L149 (1989)
 - ¹⁷ F. Ritort and P. Sollich, *Adv. Phys.* **52**, 219 (2003)
 - ¹⁸ J. P. Garrahan, P. Sollich, and C. Toninelli, *Dynamical heterogeneities in glasses, colloids and granular media*, edited by L. Berthier, G. Biroli, J.-P. Bouchaud, L. Cipelletti, and W. van Saarloos (Oxford University Press) (2011)
 - ¹⁹ D. Chandler and J. P. Garrahan, *Annu. Rev. Phys. Chem.* **61**, 191 (2010)
 - ²⁰ S.-i. Sasa, *Phys. Rev. Lett.* **109**, 165702 (2012)
 - ²¹ G. L. Hunter and E. R. Weeks, *Rep. Prog. Phys.* **75**, 066501 (2012)
 - ²² R. Mari, F. Krzakala, and J. Kurchan, *Phys. Rev. Lett.* **103**, 025701 (2009)
 - ²³ R. Mari and J. Kurchan, *J. Chem. Phys.* **135**, 124504 (2011)
 - ²⁴ P. Charbonneau, Y. Jin, G. Parisi, and F. Zamponi, *Proc. Natl. Acad. Sci.* **111**, 15025 (2014)
 - ²⁵ K. A. Fichtorn and M. Scheffler, *Phys. Rev. Lett.* **84**, 5371 (2000)
 - ²⁶ Ajay and R. G. Palmer, *J. Phys. A* **23**, 2139 (1990)
 - ²⁷ P. Harrowell, *Phys. Rev. E* **48**, 4359 (1993)
 - ²⁸ See supplemental material at <http://apricot.ap.polyu.edu.hk/dplm> for videos showing particle dynamics in small-scale simulations at $T = 0.5$ and $T = 0.16$.
 - ²⁹ C.-H. Lam, arXiv:1508.03153 (2015)
 - ³⁰ M. Brummelhuis and H. Hilhorst, *J. Stat. Phys.* **53**, 249 (1988)
 - ³¹ W. Phillips, *Rep. Prog. Phys.* **50**, 1657 (1987)
 - ³² C.-H. Lam, arXiv:1611.03586 (2016)
 - ³³ K. Binder, *Zeitschrift für Physik* **267**, 313 (1974)
 - ³⁴ M. Toda, R. Kubo, and N. Saito, *Statistical physics I: equilibrium statistical mechanics* (Springer, Heidelberg, 1991)
 - ³⁵ A. Bortz, M. Kalos, and J. Lebowitz, *Journal of Computational Physics* **17**, 10 (1975)
 - ³⁶ C.-H. Lam, M. Lung, and L. M. Sander, *Journal of Scientific Computing* **37**, 73 (2008)
 - ³⁷ B. Derrida, *Phys. Rev. Lett.* **45**, 79 (1980)
 - ³⁸ F. Ritort, *Phys. Rev. Lett.* **75**, 1190 (1995)
 - ³⁹ M. Newman and C. Moore, *Phys. Rev. E* **60**, 5068 (1999)